Effects of Swelling Agents on the Crystallization Behavior and Mechanical Properties of Polyamide 6/Clay Nanocomposites

Chen-Chi M. Ma, Chun-Ting Kuo, Hsu-Chiang Kuan, Chin-Lung Chiang

Institute of Chemical Engineering, National Tsing Hua University, Hsin-chu 30043, Taiwan, Republic of China

Received 3 January 2002; accepted 28 July 2002

ABSTRACT: Montomorillonite was organically modified with three different swelling agents: *n*-dodecylamine, 12-aminolauric acid, and 1,12-diaminodecane. These organoclays and polyamide 6 (PA6) were blended in a formic acid solution. X-ray diffraction analysis showed that the clay still retained its layer structure in the PA6/clay nanocomposite. Consequently, these materials were intercalated nanocomposites. The effects of the swelling agent and organoclay content on the crystallization behavior of the PA6/clay nanocomposites were studied with differential scanning calorimetry. The results showed that the position and width of the exothermic peak of the PA6/clay nanocomposites were changed during the nonisothermal crystallization process. The clay behaved as a nucleating agent and enhanced the crystallization rate of PA6.The crystallinity of PA6 decreased with an increasing clay content. Different swelling agents also affected the crystallization behavior of PA6. The effects of the type and content of the swelling agent on the tensile and flexural properties of PA6/clay nanocomposites were also investigated. © 2003 Wiley Periodicals, Inc. J Appl Polym Sci 88: 1686–1693, 2003

Key words: nanocomposites; polyamides; clay; swelling; crystallization; mechanical properties

INTRODUCTION

Polymer composites have widely been used in the areas of electronics, transportation, construction, consumer products, and so forth. They offer unusual combinations of stiffness and toughness that are difficult to obtain from individual components. Polymer nanocomposites are defined by the particle size of the dispersed phase, which is characterized by having at least one dimension of less than 100 nm.[1] Because of the nanocscale feature, nanocomposites exhibit excellent physical, mechanical, and thermal properties in comparison with their conventional microcomposite counterparts.

There are several approaches to the preparation of polymer/clay nanocomposites, such as exfoliation adsorption,[2,3] *in situ* intercalative polymerization,[4] and melt intercalation.[5,6] Depending on the nature of the components used (layered clay, swelling agent, and polymer matrix), three main types of composites may be obtained when layered clay is added to a polymer matrix: conventional composites, intercalated nanocomposites, and exfoliated nanocomposites.[7] The interlayer spacing of the layered clay in the polymer matrix affects the physical and mechanical properties of the polymer/clay nanocomposites.

Correspondence to: C. C. M. Ma (ccma@che.nthu.edu.tw).

Journal of Applied Polymer Science, Vol. 88, 1686–1693 (2003)
© 2003 Wiley Periodicals, Inc.

Polyamide 6 (PA6) is a semicrystalline polymer material with low cost and high performance; it is currently used in fiber-reinforced thermal plastic composites in many applications. There are two major crystalline forms of PA6: α and γ.[8,9] The α form consists of fully extended planar zigzag chains, in which the adjacent antiparallel chains are joined by hydrogen bonds, and it is the most stable crystalline form thermodynamically. The α form can be obtained by slow cooling from the polymer melt. The γ form is composed of pleated sheets of parallel chains joined by hydrogen bonds, and it is less stable. It can be obtained by fast cooling from the melt or by fiber spinning at a high speed. The γ form can be converted into the α form by melting followed by recrystallization, by annealing at 160°C in a saturated steam atmosphere without any significant loss of orientation, and by the application of stress at room temperature.[10–12]

The modification of clay with swelling agents in polymer/clay nanocomposites consists of enlarging the interlayer spacing of silicate sheets and modifying the hydrophilic clay into a hydrophobic clay for better compatibility with polymers. Eventually, it can affect the properties of the final products. Different crystalline behaviors also result in different morphological properties of polymers and lead to different physical and mechanical properties. The aim of this study was to investigate the effects of swelling agents on the crystallization behavior and mechanical properties of PA6/clay nanocomposites.

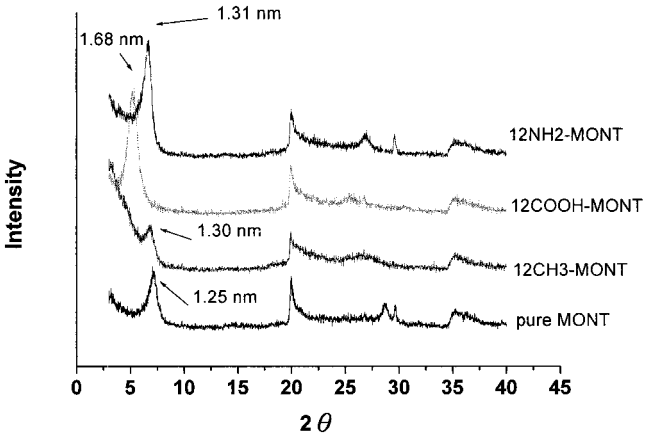

Figure 1 X-ray diffraction patterns of various organically modified montmorillonites.

EXPRIMENTAL

Materials

The clay, PK802 [Na^+-montmorillonite (MMT); cationic exchange capacity (CEC) = 77 mequiv/100 g], was obtained from Paikong Ceramic Materials Co., Ltd. (Taipei, Taiwan). PA6 was supplied by Polyscience, Inc. (Warrington, PA; molecular weight = 16,000). *n*-Dodecylamine [$NH_2(CH_2)_{11}CH_3$ (12CH3); Lancaster Synthesis Co., Ltd., Lancashire, UK], 1,12-diaminododecane [$NH_2(CH_2)_{11}NH_2$ (12NH2); Tokyo Chemical Industry Co., Ltd., Tokyo, Japan], 12-aminolauric acid [$NH_2(CH_2)_{11}CH_3$ (12COOH); Tokyo Chemical Industry], and formic acid (FA; >99%; Acros Co., Pittsburgh, PA) were used as received without further purification.

Modification of clay

A clay suspension (200 mL) with 10 g of PK802 was gradually added to 800 mL before the preparation of a solution containing 2.4 mL of HCl and 15.4 mmol of a swelling agent, and it was stirred vigorously at 60°C for 1 h. The treated montmorillonite was washed with deionized water repeatedly until no precipitate of AgCl was formed, whereas the filtrate was titrated with a 0.1*N* $AgNO_3$ solution so that the complete removal of chloride ions would be ensured. The filter cake was then dried in a vacuum oven at 80°C for 1 day for drying. The dried cake was ground and screened with a 325-mesh sieve so that organoclays would be obtained. These organoclays were denoted MONT, 12CH3–MONT, 12COOH–MONT, and 12NH2–MONT.

TABLE I
***d* Values of Organoclays Modified with Various Swelling Agents**

Clay type	*d*-spacing (nm)
MONT	1.25
12CH3–MONT	1.30
12COOH–MONT	1.68
12NH2–MONT	1.31

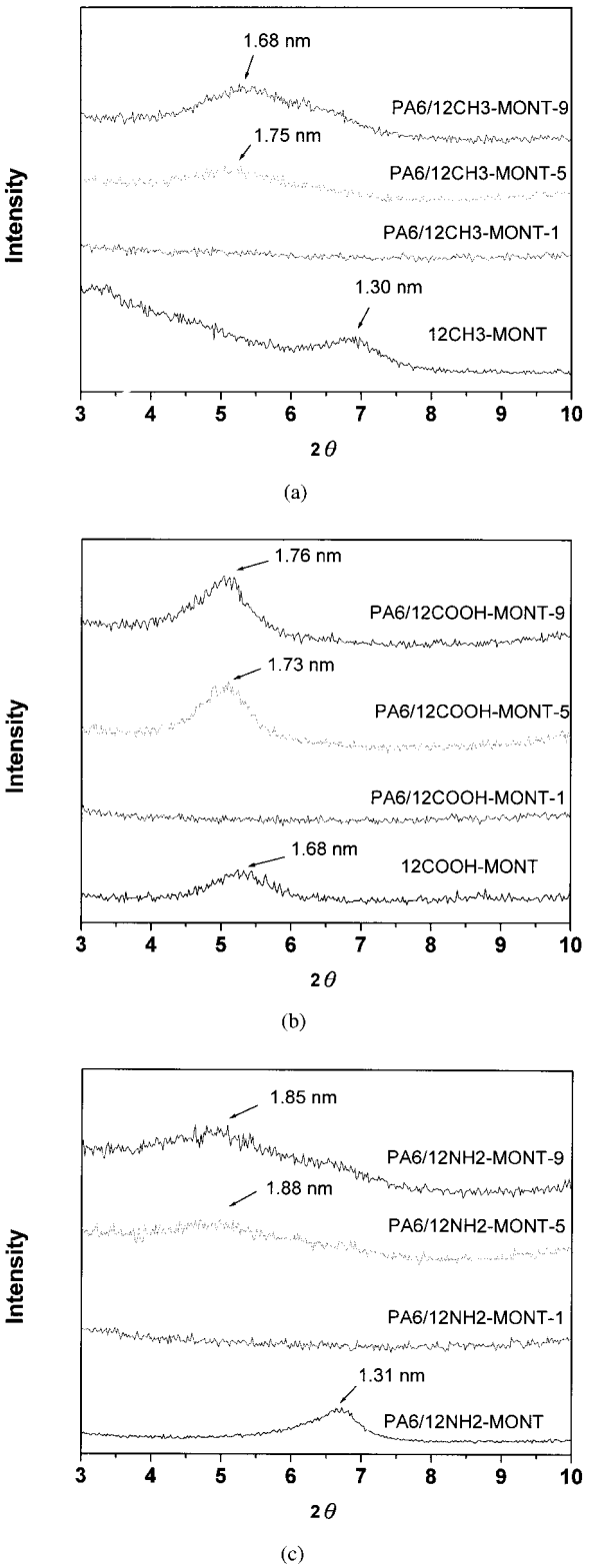

Figure 2 X-ray diffraction patterns of (a) PA6/12CH3–MONT nanocomposites, (b) PA6/12COOH–MONT nanocomposites, and (c) PA6/12NH2–MONT nanocomposites with various organoclay contents.

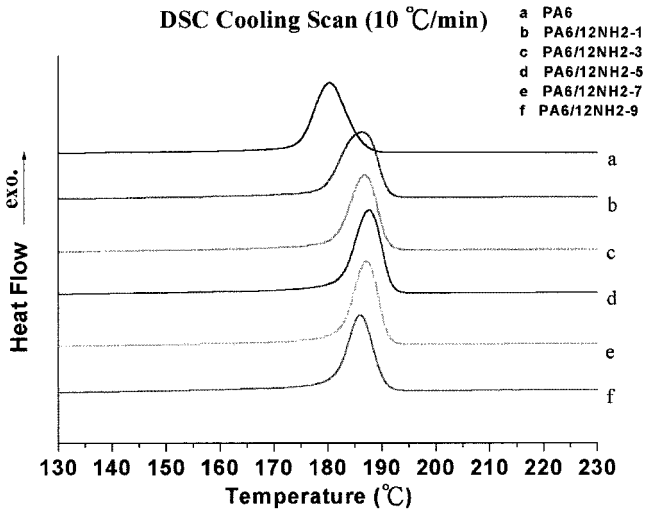

Figure 3 DSC curves of PA6/12NH2–MONT nanocomposites with various organoclay contents.

Preparation of the PA6/clay nanocomposites

Different amounts of organoclays [1, 3, 5, 7, and 9 parts per hundred parts of polymer resin (phr)] were added to a 5 wt % PA6/FA solution and vigorously stirred for 6 h. The solution was poured into deionized water, and the fibrous PA6/clay nanocomposite was obtained. The fibrous material was washed several times with deionized water for the removal of FA and then washed with methanol several times for the removal of residual water. The product were then placed in a vacuum oven at 40°C for 24 h. These PA6/clay nanocomposites were denoted PA6/organoclay-*n*, where *n* represents the amount of clay in the composite (phr).

TABLE II
T_m and T_c of Various PA6/Clay Nanocomposites During Melt Crystallization

		Clay content (phr)					
Property	Specimen	0	1	3	5	7	9
T_c (°C)	PA6/12CH3	180.3	184.4	184.8	184.5	185.2	184.8
	PA6/12COOH	180.3	186.3	184.0	183.3	184.3	184.5
	PA6/12NH2	180.3	186.2	186.8	187.6	187.1	186.0
T_m (°C)	PA6/12CH3	219.9	219.5	219.5	219.3	219.2	219.0
	PA6/12COOH	219.9	219.4	219.4	219.6	218.8	218.4
	PA6/12NH2	219.9	219.3	218.8	218.4	218.6	218.4

Characterization

Wide-angle X-ray diffraction (WAXD)

The samples were placed in a vacuum oven at 105°C for 24 h before being tested. The samples were then placed on a aluminum plate, preheated to 250°C for 10 min, and slowly cooled to room temperature. An X-ray analysis was obtained on an X-ray diffractometer equipped with Cu Kα radiation (model Lt-801, Scintag, Inc., Santa Clara, CA) at a scan rate of 4°/min from $2\theta = 3°$ to $2\theta = 10°$. Bragg's law, $\lambda = 2d \sin \theta$, was used to calculate the interlayer spacing (d).

Differential scanning calorimetry (DSC)

The samples were first placed in a vacuum oven at 100°C for 24 h before being sealed in an aluminum sample cell. For melt crystallization, the samples were kept at 250°C for 10 min, cooled to room temperature at a cooling rate of 10°C/min, and then heated to 250°C at a heating rate of 20°C/min. For cold crystallization, samples were first placed at 250°C for 10 min and then quickly put into liquid nitrogen so that amorphous samples would be obtained. These amorphous

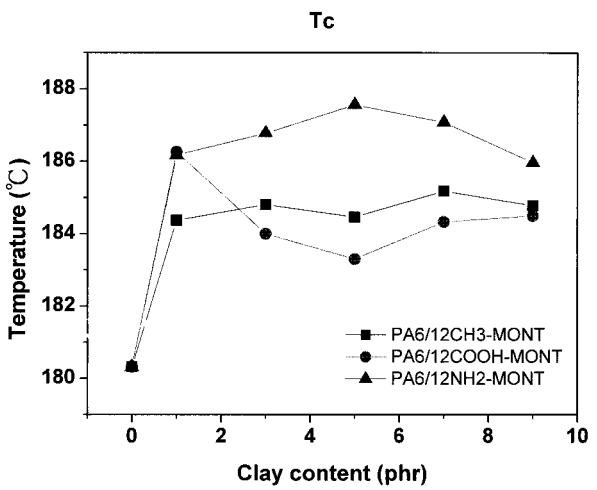

Figure 4 Effect of the clay content on the exothermic peak temperature of PA6/clay nanocomposites during melt crystallization (cooling rate = 10°C/min).

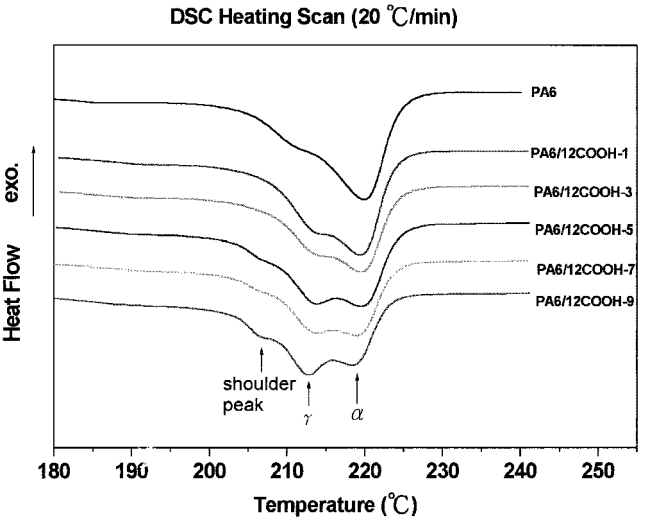

Figure 5 DSC curves of PA6/12COOH–MONT nanocomposites with various organoclay contents.

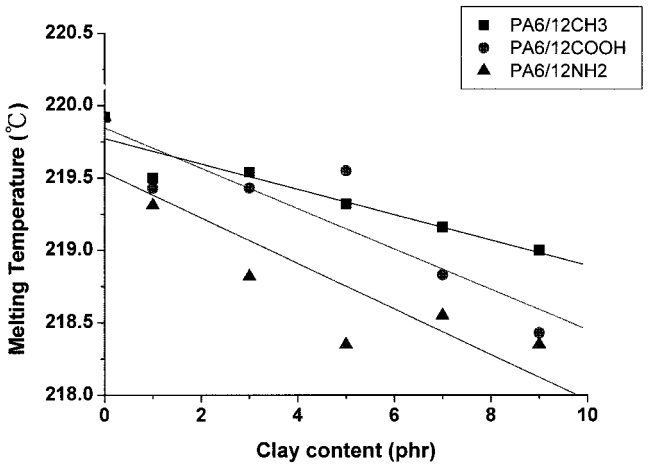

Figure 6 Melting points of PA6/clay nanocomposites with various organoclay contents (melt-crystallized; heating rate = 20°C/min).

samples were heated again to 250°C at a heating rate of 20°C/min. All data were obtained on a TA Instruments DSC 10 (DuPont, New Castle, DE).

Mechanical properties

The samples were prepared with the following procedure. Various amounts of organoclays (1, 3, 5, 7, and 9 phr) were mixed with polyamide pellets in a plasticating extruder (single screw) at a rotation speed of 20 rpm; the temperature profiles were 190–210–230–220°C (for each zone). Extruded material was cut into small pellets in a granulator and then injection-molded at a molding temperature of 235°C and at a pressure of 13.5 MPa for the preparation of dumbbell-shaped specimens.

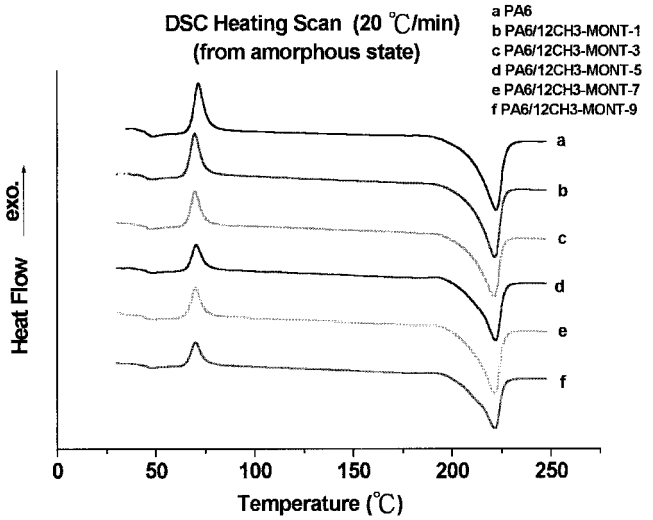

Figure 7 DSC curves of quenched PA6/12CH3–MONT nanocomposites with various organoclay contents (heating rate = 20°C/min).

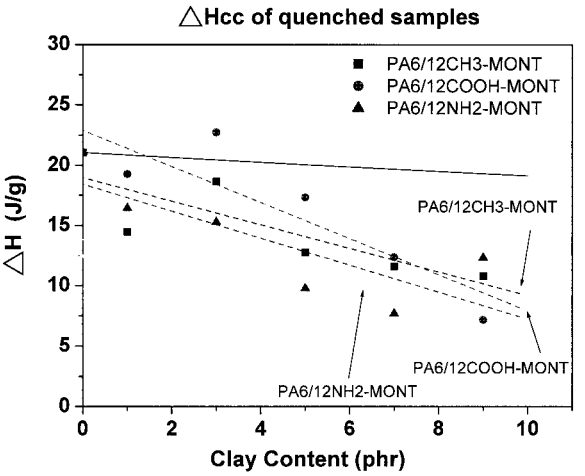

Figure 8 Effects of the clay content on ΔH_{cc} of PA6/clay nanocomposites (heating rate = 20°C/min).

The tensile tests were performed in an Instron test machine (model 4468, Instron, Inc., Canton, MA) at room temperature. The samples were measured according to ASTM D 638 at a crosshead speed of 20 mm/min. A Testometric Micro 500 machine (Rochdale, UK) was used to measure the flexural strength and flexural modulus of the specimens with a span-to-depth ratio of 40 and a crosshead speed of 1.0 mm/min according to ASTM D 90. The notched impact strength was tested according to ASTM D 256, and a TMI testing machine (TMI Co., Amityville, NY) was used (the dimensions of these samples were 63.0 mm × 12.7 mm × 3.2 mm (length × width × thickness).

RESULTS AND DISCUSSION

WAXD analysis

Figure 1 displays the WAXD patterns of pristine MONT, 12CH3–MONT, 12COOH–MONT, and 12NH2–MONT.

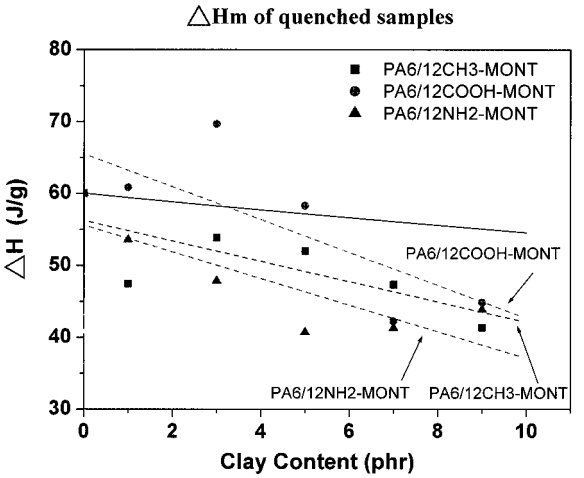

Figure 9 Effects of the clay content on ΔH_m of PA6/clay nanocomposites (heating rate = 20°C/min).

TABLE III
ΔH_{cc}, ΔH_m, and T_m of Various PA6/Clay Nanocomposites During Cold Crystallization

Property	Specimen	Clay content (phr)					
		0	1	3	5	7	9
ΔH_{cc} (J/g)	PA6/12CH3	21.1	14.5	18.6	12.8	11.6	10.8
	PA6/12COOH	21.1	19.3	22.7	17.3	12.4	7.2
	PA6/12NH2	21.1	16.4	15.3	9.8	7.7	12.3
ΔH_m (J/g)	PA6/12CH3	60.0	47.5	53.9	52.0	47.4	41.4
	PA6/12COOH	60.0	60.8	69.7	58.3	42.3	44.9
	PA6/12NH2	60.0	53.6	47.9	40.7	41.3	43.9
T_m (°C)	PA6/12CH3	222.3	221.6	221.3	222.0	221.4	221.7
	PA6/12COOH	222.3	222.0	220.4	221.6	220.8	220.9
	PA6/12NH2	222.3	221.7	221.5	221.8	221.9	221.7

A clear diffraction peak, representing the ⟨001⟩ peak of montmorillonite at 2θ = 5–8°, can be observed. Table I shows the interlayer spacing data for pristine MONT, 12CH3–MONT, 12COOH–MONT, and 12NH2–MONT (according to Bragg's equation, $d = \lambda/2 \sin \theta$); the interlayer spacings of MONT, 12CH3–MONT, 12COOH–MONT, and 12NH2–MONT were 1.25, 1.30, 1.68, and 1.31 nm, respectively. The smallest *d*-spacing of 12CH3–MONT resulted from the smallest dimension of the —CH_3 group among the three end groups. The largest *d*-spacing of 12 COOH–MONT may be attributed to the largest dimension of the —COOH group. Furthermore, both the silicate layer and the —COOH group, carrying negative charges during the preparation of the organoclay, also contributed to the largest *d*-spacing.

Figure 2(a–c) shows the WAXD patterns of PA6/12CH3–MONT, PA6/12COOH–MONT, and PA6/12NH2–MONT nanocomposites, respectively. The PA6/clay nanocomposites prepared in this study were determined to be intercalated nanocomposites by the presence of the ⟨001⟩ peak of montmorillonite in the WAXD patterns.

Thermal analysis

Nonisothermal crystallization

Melt crystallization. Nonisothermal crystallization experiments were conducted via DSC cooling scans on the PA6 and PA6/clay nanocomposites at a cooling rate of 10°C/min, and the results are shown in Figure 3. The temperatures of crystallization (T_c's) are illustrated in Figure 4 and are summarized in Table II. Only one exothermic peak temperature can be observed for each curve between 180 and 188°C. The addition of clay raised T_c by about 5–8°C, and T_c did not change very much with different clay contents. The increase in the peak temperature indicated that the clay served as a nucleating agent and increased the crystallization rate of PA6.

Figure 5 shows DSC curves of PA6/12COOH nanocomposites. The samples were cooled at a rate of 10°C/min and then heated at a rate of 20°C/min. Two major endothermic peaks can be observed in the curve of neat PA6. The higher temperature peak (ca. 221°C) represents the melting point of α-form crystal of PA6, and the lower temperature peak (ca. 210°C) resulted

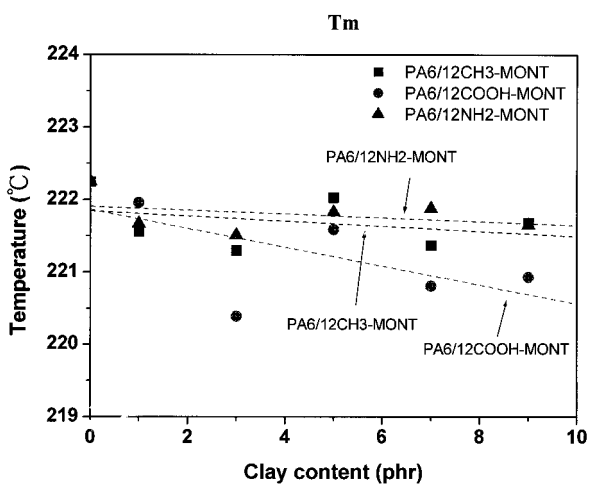

Figure 10 Effects of the clay content on T_m of PA6/clay nanocomposites during cold crystallization (heating rate = 20°C/min).

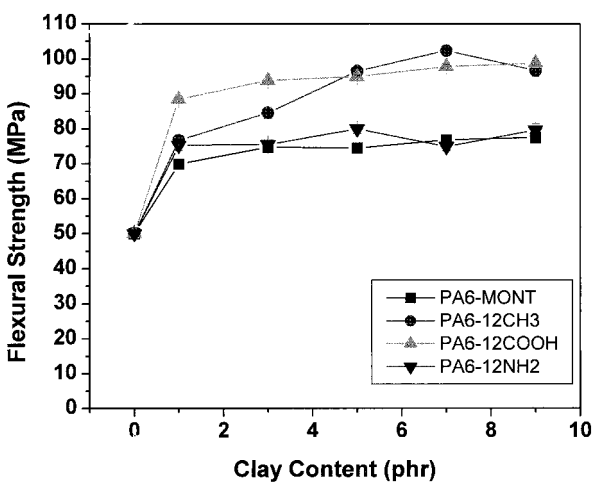

Figure 11 Effects of the organoclay contents on the flexural strength of PA6/clay nanocomposites.

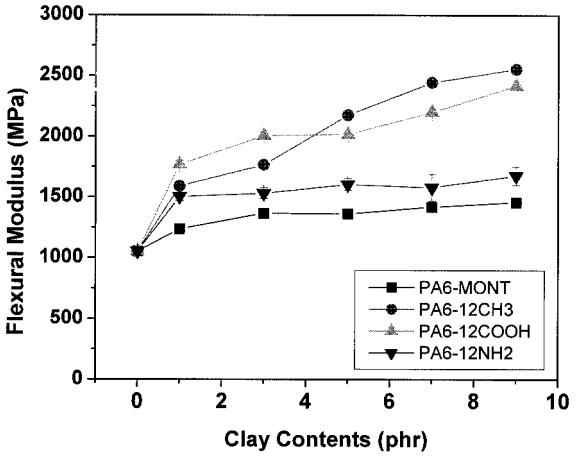

Figure 12 Effects of the organoclay contents on the flexural modulus of PA6/clay nanocomposites.

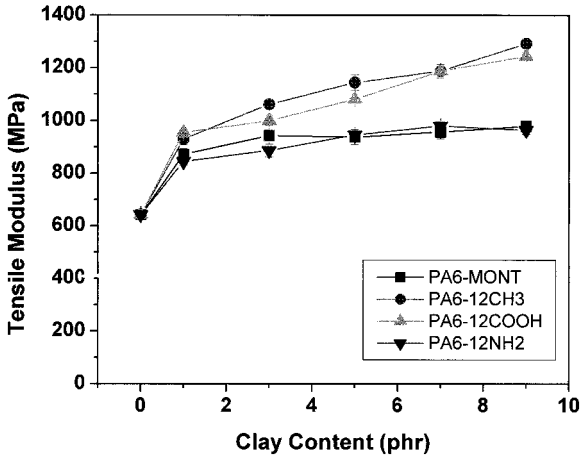

Figure 14 Effects of the organoclay contents on the tensile modulus of PA6/clay nanocomposites.

from imperfect crystals. With the addition of clay, the lower temperature peak disappeared, and a new peak formed at 213°C, indicating the formation of γ-form crystals of PA6. As the clay content increased, the content of γ-form crystals increased; this showed that the presence of clay enhanced the formation of γ-form crystals.

A new shoulder peak appeared at 205–210°C in PA6/12COOH–MONT with an increasing clay content. The shoulder peak might have resulted from the meeting of unstable crystals of smaller or imperfect crystallites formed during the cooling scan or heating scan. However, this phenomenon was not observed in PA6/12CH3–MONT and PA6/12NH2–MONT nanocomposites. The swelling agents used in this study were aliphatic amines with different end groups: —CH_3, —COOH, and —NH_2. Among them, the —COOH and —NH_2 groups showed stronger interactions with the PA6 molecule than the —CH_3 group. The presence of stronger interactions might have restricted the mobility of the polymer chains of PA6 when the crystallization process took place, resulting in the formation of small, imperfect crystallites with lower melting temperatures (T_m's). However, the same phenomenon was not observed in the PA6/12NH2–MONT nanocomposites. This might have been due to the two ends of 12NH2 being attached to the clay surface through ionic bonding during the clay modification process and resulting in a lower fraction of —NH_2 groups in the PA6/12NH2–MONT nanocomposites. Consequently, the interactions between the —NH_2 group and PA6 were reduced.

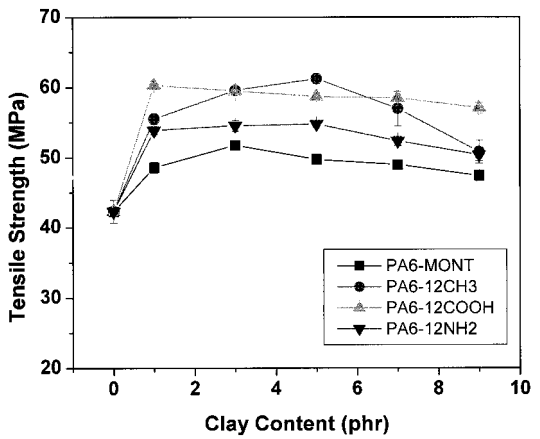

Figure 13 Tensile strength of PA6/12COOH–MONT nanocomposites.

T_m's of α-form crystals of each PA6/clay nanocomposite are plotted in Figure 6 and listed in Table II. The results showed that the addition of clay lowered T_m of PA6, indicating that small PA6 crystallites with lower T_m's were formed because of the inhibition of clay.

Cold crystallization. The cold crystallization of amorphous PA6/clay nanocomposites was carried out at a heating rate of 20°C/min. DSC curves of PA6/12CH3–MONT nanocomposites are shown in Figure 7. The amorphous PA6 started to crystallize at temperatures above the glass-transition temperature, and an exothermic peak appeared. This peak was the primary crystallization region,[9] and the heat released during this region was denoted ΔH_{cc}, the enthalpy of cold crystallization. Further crystallization took place at the end of the exothermic peak until the melting process began. The crystallization that occurred in this region was defined as the secondary crystallization.[13] Therefore, the enthalpy of melting (ΔH_m) should be equal to the sum of the heat released during the primary and secondary crystallization regions. The values of ΔH_m and ΔH_{cc} of each PA6/clay nanocomposite are shown in Figures 8 and 9 and are summarized in Table III. ΔH_{cc} was about two-thirds of ΔH_m, and this indicated that a large fraction of the crystals of PA6 formed in the secondary crystallization region. Figure 9 shows the effect of the clay content on ΔH_m of PA6/clay

TABLE IV
Mechanical Properties of PA6/MONT Nanocomposites

Clay content (phr)	Flexural strength (MPa)	Flexural modulus (MPa)	Tensile strength (MPa)	Tensile modulus (MPa)	Izod impact strength (notched; ft lb/in.)
0	50.0	1052.6	42.3	642.0	1.31
1	69.9 (40)	1237.6 (18)	48.6 (36)	871.4 (36)	1.665 (27)
3	74.8 (50)	1366.6 (30)	51.8 (47)	943.2 (47)	1.686 (29)
5	74.4 (49)	1362.9 (29)	49.7 (46)	937.3 (46)	1.797 (37)
7	76.8 (54)	1419.6 (35)	49.0 (49)	957.0 (49)	1.811 (38)
9	77.5 (55)	1458.1 (39)	47.4 (52)	978.6 (52)	1.817 (39)

The numbers in parentheses represent the percentage increase in mechanical properties compared to neat PA6.

nanocomposites. A solid line is drawn in Figure 9 through the values of ΔH_{cc} of neat PA6 and PA6/organoclay-100 (under the assumption that the enthalpy of the clay was 0). Almost all values of the PA6/organoclay nanocomposites are under the solid line. The higher the clay content was, the lower the crystallinity was of PA6; therefore, the addition of clay might have reduced the crystallinity of PA6. This phenomenon might have resulted from the clay restricting the chain mobility of PA6 and leading to lower crystallinity.

The T_m values of each PA6/clay nanocomposite are illustrated in Figure 10 and are also listed in Table III. Only one melting peak was found at 220°C; this indicated that only the α-form crystal formed during the cold crystallization. This phenomenon was different from the melt crystallization. In the melt crystallization, two melting peaks of α- and γ-form crystals of PA6 could be observed. The addition of clay lowered T_m of PA6, and this implied that small PA6 crystallites formed in the presence of clay.

Mechanical properties

Figures 11–14 show the mechanical properties of PA6/clay nanocomposites. Adding a small amount of clay increased the mechanical properties very significantly. The types of swelling agents affected the mechanical properties. Although adding untreated montmorillonite could slightly increase the mechanical properties of PA6, the addition of treated montmorillonite, that is, 12CH3–MONT, 12COOH–MONT, or 12-NH2–MONT, enhanced the properties significantly. Figures 11–14 show the effects of the clay content and the type of swelling agent on the flexural strength, modulus, and tensile strength of the nano-

TABLE V
Mechanical Properties of PA6/12CH3–MONT Nanocomposites

Clay content (phr)	Flexural strength (MPa)	Flexural modulus (MPa)	Tensile strength (MPa)	Tensile modulus (MPa)	Izod impact strength (notched; ft lb/in.)
0	50	1052.6	42.3	642	1.31
1	76.7 (53)	1590.3 (51)	55.5 (31)	929.5 (45)	2.80 (114)
3	84.5 (69)	1765.4 (68)	59.6 (41)	1061.0 (65)	2.00 (53)
5	96.5 (93)	2176.7 (107)	61.2 (45)	1143.9 (78)	1.97 (50)
7	102.3 (105)	2446.3 (132)	57.0 (35)	1188.0 (85)	1.39 (6)
9	96.7 (93)	2556.0 (143)	50.8 (20)	1292.8 (101)	1.26 (−4)

The numbers in parentheses represent the percentage increase in mechanical properties compared to neat PA6.

TABLE VI
Mechanical Properties of PA6/12COOH–MONT Nanocomposites

Clay content (phr)	Flexural strength (MPa)	Flexural modulus (MPa)	Tensile strength (MPa)	Tensile modulus (MPa)	Izod impact strength (notched; ft lb/in.)
0	50.0	1052.6	42.3	642	1.31
1	88.5 (77)	1768.4 (68)	60.3 (43)	954 (49)	1.71 (28)
3	93.8 (88)	2007.2 (91)	59.5 (19)	999 (56)	0.92 (−29)
5	94.9 (90)	2019.1 (92)	58.7 (17)	1081 (69)	0.97 (−26)
7	97.8 (96)	2201.3 (109)	58.5 (17)	1188 (85)	0.99 (−24)
9	98.8 (98)	2419.5 (129)	57.1 (14)	1244 (94)	0.69 (−47)

The numbers in parentheses represent the percentage increase in mechanical properties compared to neat PA6.

TABLE VII
Mechanical Properties of PA6/12NH2–MONT Nanocomposites

Clay content (phr)	Flexural strength (MPa)	Flexural modulus (MPa)	Tensile strength (MPa)	Tensile modulus (MPa)	Izod impact strength (notched; ft lb/in.)
0	50.0	1052.6	42.3	642	1.31
1	75.3 (51)	1502.8 (43)	53.9 (27)	844.6 (32)	2.50 (91)
3	75.5 (51)	1532.0 (46)	54.5 (29)	885.6 (38)	1.87 (43)
5	80.0 (60)	1604.6 (52)	54.8 (29)	945.4 (47)	2.02 (54)
7	74.9 (50)	1580.0 (50)	52.4 (24)	979.1 (53)	1.94 (48)
9	79.6 (59)	1678.0 (59)	50.4 (19)	964.3 (50)	2.11 (61)

The numbers in parentheses represent the percentage increase in mechanical properties compared to neat PA6.

composites. The addition of a small amount of clay (up to 5 phr) could increase the tensile strength of the material; however, when the clay content was higher than 5 phr, the tensile strength decreased. The organic treatment of the clay also affected the flexural properties of the PA6/clay nanocomposite.

Tables IV–VII summarize the mechanical properties of PA6/clay nanocomposites. The numbers in the brackets represent the percentages of the increase in the mechanical properties with respect to the neat PA6. When a small amount of montmorillonite (1 phr) was added, the flexural strength increased from 40% for PA6/MONT (Table IV) to 77% for PA6/12COOH–MONT (Table VI), and the flexural modulus increased from 18% for PA6/MONT to 68% for PA6/12COOH–MONT. The maximum values of the flexural strength and flexural modulus reached 98 (Table VI) and 143% (Table V), respectively, when 9 phr clay was added. When 1 phr montmorillonite was added, the tensile strength increased from 15% for PA6/MONT to 43% for PA6/12COOH–ONT), and the tensile modulus increased from 36% for PA6/MONT to 49% for PA6/12COOH–MONT. The tensile modulus reached as high as 101% (PA6/12CH3–MONT; Table V). Table VII shows the mechanical properties of PA6/12NH2–MONT nanocomposites and indicates that the modification of clay would improve the mechanical properties of nanocomposites.

CONCLUSIONS

Three types of swelling agents were used to modify montmorillonite: 12CH3, 12COOH, and 12NH2. These organoclays and PA6 were blended in FA solutions. X-ray diffraction analysis showed that the clay still retained its layer structure in the PA6/clay nanocomposites. Consequently, these materials were intercalated nanocomposites. The effects of the swelling agent and the organoclay content on the crystallization behavior of the PA6/clay nanocomposites were studied with DSC. Only one exothermic peak was found in both melt and cold crystallization. Two melting peaks were observed in the melt crystallization, indicating that the addition of clay induced the formation of γ-form crystals of PA6. However, only one melting peak was found in the cold crystallization samples. The crystallization peak in the melt crystallization arose around 5°C and implied that clay behaved as a nucleating agent and enhanced the crystallization rate of PA6.The crystallinity of PA6 decreased with increasing clay content because of clay inhibiting the chain mobility. The overall crystallinity was reduced from 35 to 26% when 9 phr organoclay was added. The addition of clay lowered the melting point of PA6 because of the formation of imperfect crystals. The results also showed that, during cold crystallization, about two-thirds of the crystals were formed. A small amount (5 phr) of clay could increase the tensile and flexural properties of PA6 significantly. The montmorillonite treated with a swelling agent could improve both the tensile and flexural properties of PA6/clay nanocomposites significantly.

References

1. Gianellis, E. P. Adv Mater 1996, 8, 29.
2. Ogata, N.; Kawakage, S.; Ogihara, T. J Appl Polym Sci 1997, 66, 573.
3. Jimenez, G.; Ogata, N.; Kawai, H.; Ogihara, T. J Appl Polym Sci 1997, 64, 2211.
4. Kojima, Y.; Usuki, A.; Kawasumi, M.; Okada, A.; Kurauchi, T.; Kamigaito, O. J Polym Sci Part A: Polym Chem 1993, 31, 1755.
5. Liu, L.; Qi, Z.; Zhu, X. J Appl Polym Sci 1999, 71, 1133.
6. Vaia, R. A.; Jandt, K. D.; Kramer, E. J.; Giannelis, E. P. Chem Mater 1996, 8, 2628.
7. Alexandre, M.; Dubois, P. Mater Sci Eng 2000, 28, 1.
8. Miyasaka, K.; Ishikawa, K. J Polym Sci Part A-2: Polym Phys 1972, 10, 1497.
9. Miyasaka, K.; Ishikawa, K. J Polym Sci Part A-2: Polym Phys 1968, 6, 1317.
10. Holmes, D. R.; Bunn, C. W.; Smith, D. J. J Polym Sci 1955, 17, 159.
11. Arimoto, H.; Ishibashi, M.; Hirai, M.; Chatani, T. J Polym Sci Part A: Gen Pap 1965, 3, 317.
12. Hiramatsu, N.; Hirakawa, S. Polym J 1982, 14, 165.
13. Khanna, Y. P.; Kuhn, W. P. J Polym Sci Part B: Polym Phys 1997, 35, 2219.
14. Park, C. I.; Park, O. O.; Lim, J. G.; Kim, H. J. Polymer 2001, 42, 7465.
15. Yoon, J. T.; Jo, W. H.; Lee, M. S.; Ko, M. B. Polymer 2001, 42, 329.
16. Hambir, S.; Bulakh, N.; Kodgire, P.; Kalgaonkar, R.; Jog, J. P. J Polym Sci Part A: Polym Chem 2001, 39, 446.